Measuring Gaussian noise using a lock-in amplifier

T. Kouh
Mechanical Engineering Department and the Photonics Center, Boston University, Boston,
Massachusetts 02215 and Department of Physics, Kookmin University, Seoul 136-702, South Korea

U. Kemiktarak
Joint Quantum Institute, University of Maryland, College Park, Maryland 20742 and National Institute of
Standards and Technology, Gaithersburg, Maryland 20899

O. Basarir, C. Lissandrello, and K. L. Ekinci[a)]
Mechanical Engineering Department and the Photonics Center, Boston University, Boston,
Massachusetts 02215

Gaussian fluctuations (or Gaussian noise) appear in almost all measurements in physics. Here, a concise and self-contained introduction to thermal Gaussian noise is presented. Our analysis in the frequency domain centers on thermal fluctuations of the position of a particle bound in a one-dimensional harmonic potential, which in this case is a microcantilever immersed in a bath of room-temperature gas. Position fluctuations of the microcantilever, detected by the optical beam deflection technique, are then fed into a lock-in amplifier to measure the probability distribution and spectral properties of the fluctuations. The lock-in amplifier measurement is designed to emphasize the frequency-domain properties of Gaussian noise. The discussion here can be complementary to a discussion of Gaussian fluctuations in the time domain. © *2014 American Association of Physics Teachers.*
[http://dx.doi.org/10.1119/1.4873694]

I. INTRODUCTION

When a small particle is immersed in a liquid, it displays an irregular and random motion. This phenomenon, called "Brownian motion,"[1] is caused by the thermal fluctuations in a system with a large number of degrees of freedom. The Brownian particle is incessantly bombarded by the liquid molecules, each of which has a small amount of thermal energy $\sim k_B T$, with k_B being the Boltzmann constant and T being the absolute temperature. Similar are the random oscillations of a cantilever in a bath of fluid[2] or the fluctuating voltage across a resistor,[3] both under thermal equilibrium. Although these thermal phenomena are easily observable,[3,4] a deeper understanding of them requires delving into the theory of random processes and realizing the central importance of the Gaussian distribution in the formulation of thermal fluctuations.

The reason for using the Gaussian distribution for describing thermal phenomena is that thermal fluctuations come from a large number of almost independent events.[5] The Gaussian law of errors[5] states that, if the error in an observable is due to the accumulation of a large number of small uncertainties, the error follows a Gaussian distribution.[6] Returning to the Brownian particle, we realize that at any given instant, the particle is buffeted by an enormous number of molecules. The net force on the particle comes from the resultant of these molecular buffeting forces and fluctuates at a time scale much faster than the particle can respond. Hence, the force can be considered to be Gaussian distributed around a zero mean at each instant. Furthermore, if the thermal force is Gaussian, the response of any linear system under the action of this thermal force (the Brownian particle or the cantilever) will also be Gaussian.[5]

Much recent attention has been directed to the study of thermal fluctuations in the undergraduate laboratory. Several papers have explored thermal fluctuations in electrical circuit elements, extracting the Boltzmann constant from the measurements of electrical quantities.[3,7–9] More recently, the exquisite displacement sensitivity of optical techniques combined with the small spring constants of microcantilevers has brought thermal fluctuations in mechanical systems within reach.[4] In particular, Shusteff *et al.*[4] used interferometry to calibrate the displacement fluctuations of a microcantilever and determined the Boltzmann constant from thermal mechanical fluctuations. The purpose of this manuscript is to complement the existing educational literature on fluctuations and measurement techniques. While we also study the thermal fluctuations of a microcantilever, our experimental focus is not on the determination of the Boltzmann constant. Instead, our lock-in amplifier experiments are designed to emphasize the Gaussian nature of the thermal fluctuations. Furthermore, we focus on some important concepts in basic measurement science, such as frequency mixing, lock-in amplifier operation, noise and spectral measurements. The topics are complementary to the current emphasis in the undergraduate laboratory on automated data acquisition and digital signal processing (e.g., digital filtering and Fourier transforming). Finally, the experiment described here is straightforward to set up or can be based upon an existing atomic force microscope (AFM) apparatus.[10]

The outline of the article is as follows. In Sec. II, we analyze the Brownian motion of a particle bound in a harmonic potential. We derive transparent expressions for the displacement fluctuations of the particle in the frequency domain, starting with certain physical assumptions for the thermal drive force. In Sec. III, we consider how these fluctuations can be detected by a lock-in amplifier. In Sec. IV, we turn to a simple experiment that investigates the Gaussian nature of the thermal fluctuations of a Brownian particle in a harmonic potential immersed in a gas. An AFM microcantilever in atmosphere serves as our harmonically bound Brownian particle. The thermal fluctuations of the microcantilever are detected by the optical beam deflection technique and analyzed using a lock-in amplifier.[11] Finally, we provide conclusions in Sec. V.

II. THE MICROCANTILEVER: A BROWNIAN PARTICLE IN A HARMONIC POTENTIAL

A. Equation of motion

A microcantilever oscillating in its fundamental normal mode can be modeled as a particle in a one-dimensional harmonic potential, like a particle on a spring, as shown in Fig. 1(a). The particle has mass m, with a harmonic restoring force given by $-\kappa z = -m\Omega_0^2 z$. Here, z is the position of the particle, and $\kappa = m\Omega_0^2$ is the spring constant.

The microcantilever immersed in a bath of fluid (gas) in thermal equilibrium can thus be treated as a Brownian particle in a harmonic potential. The gas exerts on the microcantilever a force $F(t)$ that has a rapidly fluctuating component $R(t)$ and a slowly varying component proportional to the instantaneous velocity $\dot{z}$ of the particle.[12] The force is therefore separated as[12] $F(t) = -m\gamma\dot{z} + R(t)$ where γ is called the dissipation constant. Because both $-m\gamma\dot{z}$ and $R(t)$ originate from the surrounding gas, they are linked through the fluctuation-dissipation theorem.[13] In summary, we write

$$m\ddot{z} + m\gamma\dot{z} + m\Omega_0^2 z = R(t), \tag{1}$$

as the equation of motion describing the fluctuations of the microcantilever in a gas under thermal equilibrium.

The system under study here is a lightly damped harmonic oscillator. In a lightly damped system the resonance frequency will remain, for all practical purposes, identical to the undamped resonance frequency $\Omega_0/2\pi$. Light damping can be characterized in terms of the quality factor of resonance Q, which is defined as $Q = \Omega_0/\gamma$. For $Q \geq 10$, the damped resonance frequency deviates from $\Omega_0/2\pi$ by less than 1%, so the light damping approximation becomes very accurate. The gas damping here indeed provides light damping with $Q \sim 100$. Driven by a random thermal force, a lightly-damped harmonic oscillator will undergo oscillations (when observed in the time domain).[14] These "random oscillations" with frequency $\Omega_0/2\pi$ tend to persist, on the average, for a number of Q cycles. The oscillations therefore remain coherent for a time interval $\sim 2\pi Q/\Omega_0$, providing a correlation time for the system dynamics.

B. Thermal force

The fluctuating component of the thermal force $R(t)$ results from numerous gas molecule impacts so that the
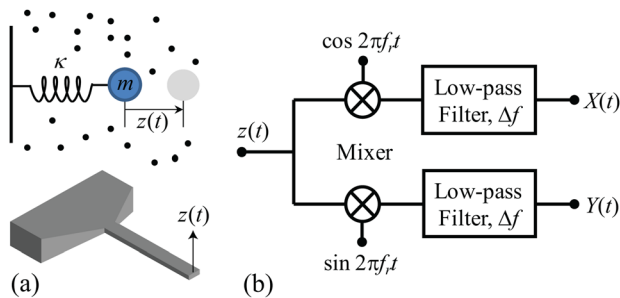

Fig. 1. (a) A microcantilever oscillating at a frequency close to its fundamental resonance frequency can be modeled as a harmonically-bound particle with mass m. The stiffness of the spring is κ. (b) Block diagram of a lock-in amplifier. The input signal $z(t)$ is separated into two channels and mixed with sinusoidal reference signals. After mixing, both channels are low-pass filtered, resulting in the so-called in-phase $X(t)$ and quadrature-phase $Y(t)$ components of $z(t)$.

Gaussian property holds by the central limit theorem. We first introduce ensemble averaging. Ensemble averages are taken over identically prepared systems existing in different states at a *fixed* instant in time.[15] To take ensemble averages, we use the probability distribution $\mathcal{P}(R; t)\,dR$, which quantifies the probability that $R(t)$ lies in the interval $R \leq R(t) \leq R + dR$ at time t. It follows that

$$\langle R(t)\rangle \equiv \int_{-\infty}^{\infty} R\,\mathcal{P}(R; t)\,dR, \tag{2}$$

$$\langle R^2(t)\rangle \equiv \int_{-\infty}^{\infty} R^2\,\mathcal{P}(R; t)\,dR, \tag{3}$$

and so on. While $R(t)$ itself is random, qualitatively it remains the same over time. It can be deduced that $\mathcal{P}(R)\,dR$ does not depend on time and is given by[5]

$$\mathcal{P}(R)\,dR = \frac{e^{-R^2/2\sigma_R^2}}{\sigma_R\sqrt{2\pi}}\,dR, \tag{4}$$

where σ_R^2 is the variance. Thus, σ_R is the standard deviation, which quantifies the root mean square (r.m.s.) fluctuation amplitude of $R(t)$. In the special case when $\mathcal{P}(R; t) = \mathcal{P}(R)$, the random Gaussian physical quantity is called stationary. For a stationary random variable such as $R(t)$, long time averages and ensemble averages provide the same outcome. This is because, in a long time interval, the fluid bath giving rise to $R(t)$ is expected to sample all possible states. Finally, we expect $\langle R(t)\rangle = 0$ and $\langle R^2(t)\rangle = \langle R^2(t+s)\rangle = \sigma_R^2$ for all t and s.[16]

Considering the force $R(t)$ for a long time $\mathcal{T}$ and taking it to be periodic with period $\mathcal{T}$, we can expand $R(t)$ in terms of a Fourier series as[5]

$$R(t) = \sum_{n=1}^{\infty} A_n \cos \omega_n t + B_n \sin \omega_n t, \tag{5}$$

where the Fourier frequency $f_n = \omega_n/(2\pi) = n/\mathcal{T}$. The $n = 0$ term is not included because a time-average of the force over a long interval should vanish. The coefficients A_n and B_n are all assumed to be independent (uncorrelated) random Gaussian variables with average values of zero. One can find the probability that A_n and B_n are in certain ranges dA_n and dB_n as[17]

$$\mathcal{Q}_n(A_n, B_n)\,dA_n\,dB_n = \frac{e^{-(A_n^2+B_n^2)/2\sigma_{R_n}^2}}{\sigma_{R_n}\sqrt{2\pi}}\,dA_n\,dB_n, \tag{6}$$

valid for all n. It can be shown by integrating Eq. (6) that $\langle A_n\rangle = \langle B_n\rangle = \langle A_nB_n\rangle = 0$, $\langle A_kA_m\rangle = \langle B_kB_m\rangle = \langle A_kB_m\rangle = 0$ if $k \neq m$, and $\langle A_n^2\rangle = \langle B_n^2\rangle = \sigma_{R_n}^2$. The probability distribution functions $\mathcal{Q}_n$ can intuitively be understood to result from the Gaussian law of errors. If all A_n and B_n are Gaussian variables, their linear combination in Eq. (5), $R(t)$, will also be a Gaussian variable. A joint probability distribution can be obtained for all the Fourier coefficients (A_1, A_2,...; B_1, B_2,...) from the individual probability distributions as

$$\mathcal{Q}(A_1, A_2, \ldots; B_1, B_2, \ldots) = \prod_{n=1}^{\infty} \mathcal{Q}_n(A_n, B_n). \tag{7}$$

C. Particle displacement

To solve the equation of motion shown in Eq. (1), $z(t)$ is expanded in terms of its Fourier components as

$$z(t) = \sum_{n=1}^{\infty} X_n \cos \omega_n t + Y_n \sin \omega_n t, \qquad (8)$$

where X_n and Y_n can be determined uniquely from Eq. (1) in terms of the Fourier components of the force A_n and B_n as[18]

$$X_n = \frac{1}{m} \frac{(\Omega_0^2 - \omega_n^2)A_n - \gamma \omega_n B_n}{(\Omega_0^2 - \omega_n^2)^2 + \gamma^2 \omega_n^2} \qquad (9)$$

and

$$Y_n = \frac{1}{m} \frac{\gamma \omega_n A_n + (\Omega_0^2 - \omega_n^2)B_n}{(\Omega_0^2 - \omega_n^2)^2 + \gamma^2 \omega_n^2}. \qquad (10)$$

Because A_n and B_n are both Gaussian variables, so are X_n and Y_n with a probability distribution $\mathcal{W}_n(X_n, Y_n)$, similar in form to Eq. (6).

D. Spectral density

The concept of spectral density is perhaps most easily understood in terms of a fluctuating electrical quantity, as in the noise voltage across a resistor. The average noise power dissipated in the resistor is proportional to the (ensemble or time) average of the square of the voltage. The spectral density is then the distribution of this power in frequency.[19] Similarly, the average of the square of the physical quantities we deal with, $R(t)$ and $z(t)$, can be related to the power or the energy of these particular quantities [as will be seen in Eq. (15)]. To start our discussion, we square and take averages of both sides of Eq. (5) and due to the independence of the individual Gaussian variables we obtain

$$\langle R^2(t) \rangle = \sum_{n=1}^{\infty} \langle A_n^2 \rangle \langle \cos^2 \omega_n t \rangle + \langle B_n^2 \rangle \langle \sin^2 \omega_n t \rangle. \qquad (11)$$

Furthermore, we expect that $\langle \cos^2 \omega_n t \rangle = \langle \sin^2 \omega_n t \rangle = 1/2$ and $\langle A_n^2 \rangle = \langle B_n^2 \rangle$. Given that the left hand side of Eq. (11) is σ_R^2, we write

$$\sigma_R^2 = \sum_{n=1}^{\infty} \frac{\langle A_n^2 \rangle + \langle B_n^2 \rangle}{2} = \sum_{n=1}^{\infty} \sigma_{R_n}^2. \qquad (12)$$

Thus, we can express the spectral density $S_R(f)$ as

$$S_R(f)\, df \approx \sigma_{R_n}^2, \qquad (13)$$

for $f \approx f_n$ and $df \approx f_n - f_{n-1}$. The driving force in this approximation has a white (constant and frequency-independent) thermal spectrum $S_R(f) = 4m\gamma k_B T$.[15]

Typically, $S_R(f)$ is not a directly measurable quantity. On the other hand, the spectral density $S_z(f)$ and the r.m.s fluctuations of the position of the particle are two well-defined and measurable quantities. This can be found using the response function of the particle under $R(t)$ as[15]

$$S_z(f) = \frac{1}{m} \frac{4\gamma k_B T}{(4\pi^2 f^2 - \Omega_0^2)^2 + \gamma^2 4\pi^2 f^2}. \qquad (14)$$

In the experiments below, we will be integrating $S_z(f)$ in a frequency band Δf around a center frequency f_r; this provides the variance in the particle position $z(t)$ coming only from the Fourier components of $z(t)$ with frequencies in that particular frequency band. We will also refer to this quantity as z_{rms}^2. Thus, z_{rms} is the standard deviation, but in a limited frequency band. To clarify, we write

$$z_{rms}^2 = \int_{f_r - \Delta f/2}^{f_r + \Delta f/2} S_z(f)\, df. \qquad (15)$$

Returning to Eq. (12), we realize that

$$z_{rms}^2 \approx \sum_n \frac{\langle X_n^2 \rangle + \langle Y_n^2 \rangle}{2} = \sum_n \sigma_{zn}^2, \qquad (16)$$

where the summation contains only the frequencies that satisfy $f_r - \Delta f/2 \lesssim \omega_n/2\pi \lesssim f_r + \Delta f/2$. If all terms $(n = 1, \ldots, \infty)$ are included, the variance converges to the equipartition result $\int_0^{\infty} S_z(f) df = k_B T/\kappa$, where κ is the stiffness of the spring shown in Fig. 1(a).

III. LOCK-IN AMPLIFIER MEASUREMENT OF A GAUSSIAN RANDOM VARIABLE

With the above expressions in hand, we turn to lock-in detection of the thermal fluctuations of the particle position $z(t)$. First, we convert $z(t)$ to a voltage by means of an optical transducer, resulting in a voltage proportional to $z(t)$: $V_s(t) = \mathcal{R}z(t)$, where $\mathcal{R}$ represents a constant gain. In addition, some voltage noise $V_n(t)$ is inevitably added to the signal. In order to keep our expressions simple, we assume that the transducer is noiseless and that all gains are adjusted such that we obtain an overall unity gain. Thus, $z(t)$ becomes a voltage signal with the correct units.

Most lock-in amplifiers combine analog and digital electronics. Here, we present an analysis based on the simplified block diagram[11] shown in Fig. 1(b). The input signal is split into two channels and is "mixed" with two sinusoidal reference signals, $A_r \cos \omega_r t$ and $A_r \sin \omega_r t$. The mixer is assumed to be an ideal multiplier and hence multiplies the input signal by a sinusoid with a variable frequency $f_r = \omega_r/2\pi$ determined by the user. The amplitude A_r of the reference is adjusted to $A_r = \sqrt{2}$ such that we retain the unity gain. Given the form of $z(t)$ in Eq. (8), the mixers output sinusoids at angular frequencies $\omega_n - \omega_r$ and $\omega_n + \omega_r$, and the low pass filter rejects the high-frequency sinusoids. At the two output channels of the lock-in, we obtain

$$X(t) = \sum_n \frac{X_n}{\sqrt{2}} \cos(\omega_n - \omega_r)t + \frac{Y_n}{\sqrt{2}} \sin(\omega_n - \omega_r)t \quad (17)$$

and

$$Y(t) = \sum_n -\frac{X_n}{\sqrt{2}} \sin(\omega_n - \omega_r)t + \frac{Y_n}{\sqrt{2}} \cos(\omega_n - \omega_r)t. \quad (18)$$

As in Eq. (16), the summation above is *not* over all n because of the filtering. To see the implications of the filtering, we first assume that the filter is so sharp that only one Fourier component at $\omega_r = \omega_n$ is present at the output. Then we

obtain $X(t) = X_r/\sqrt{2}$ and $Y(t) = Y_r/\sqrt{2}$, where the subscript r now indicates the Fourier component at frequency $\omega_r/2\pi$.

Values for $X(t)$ and $Y(t)$ are sampled at times $t = \tau$, 2τ, $3\tau, \ldots, N\tau$ for large N (τ is the sampling time). Such sampling generates an ensemble for the Fourier components X_r and Y_r, from which averages and standard deviations can be calculated. Equations (5) and (8) indicate that the Fourier components are to be found considering the random signal for a time $\mathcal{T}$. If τ is large enough, such that $\tau \geq \mathcal{T}$, then the Fourier components measured as such can be assumed to come from identical systems but existing in different states, i.e., a statistical ensemble. Selecting τ longer than all the correlation times present in the system should ensure this property. For the harmonically bound microcantilever, τ should be greater than the ring-down (or decay) times of both the microcantilever and the low-pass filter. Thus, the set $\{X_r, Y_r\}$ $= \{X(\tau), Y(\tau); X(2\tau), Y(2\tau); \ldots; X(N\tau), Y(N\tau)\}$ created by sampling $X(t)$ and $Y(t)$ properly can be treated as an ensemble for the random variables X_r and Y_r.

When the above-described sample set from $X(t)$ and $Y(t)$ is plotted in the xy-plane, the data points will gradually fill the plane. With a total of N samples, the number of points within $\Delta x \Delta y$ of (x, y) will be given by $N\mathcal{W}_r(x, y)\Delta x\Delta y$, where $\mathcal{W}_r$ is a Gaussian probability distribution similar to Eq. (6). The standard deviation of the sample set can be linked to the r.m.s. position fluctuations and the spectral density as

$$z_{\text{rms}}^2 \approx S_z(f_r)\Delta f \approx \frac{\langle X_r^2 \rangle + \langle Y_r^2 \rangle}{2}, \quad (19)$$

where Δf is the filter bandwidth.

It is not hard to extend the above argument to a mixed down signal with several Fourier components coming from a larger lock-in filter bandwidth Δf. In Eqs. (17) and (18), the sums can be thought to contain just a few Fourier components, the frequencies of which satisfy

$$\frac{\omega_r}{2\pi} - \frac{\Delta f}{2} \lesssim \frac{\omega_n}{2\pi} \lesssim \frac{\omega_r}{2\pi} + \frac{\Delta f}{2}. \quad (20)$$

Because X_n and Y_n are random and $\omega_n - \omega_r$ provides different angular velocities for each n in the plane, $X(t)$ and $Y(t)$ will random-walk in the plane with all their statistical properties remaining the same as above. To make this statement more concrete we look at z_{rms} and $S_z(f_r)$. Squaring and averaging the sample set from $X(t)$, for instance, we obtain

$$\langle X(t)^2 \rangle \approx \sum_n \left\langle \frac{X_n^2}{2} \right\rangle \langle \cos^2(\omega_n - \omega_r)t \rangle$$
$$+ \sum_n \left\langle \frac{Y_n^2}{2} \right\rangle \langle \sin^2(\omega_n - \omega_r)t \rangle. \quad (21)$$

Considering the independence of the Fourier components and the time averages of sinusoidals, we get

$$\langle X(t)^2 \rangle \approx \sum_n \frac{\langle X_n^2 \rangle + \langle Y_n^2 \rangle}{4}, \quad (22)$$

eventually leading to

$$z_{\text{rms}}^2 \approx \langle X(t)^2 \rangle + \langle Y(t)^2 \rangle \approx S_z(f_r)\Delta f \approx \sum_n \frac{\langle X_n^2 \rangle + \langle Y_n^2 \rangle}{2}, \quad (23)$$

with the same few Fourier components under the summation.

IV. EXPERIMENT

We now turn to a description of the experiment. We measure the thermal oscillations of a commercially available AFM microcantilever (MicroMasch HQ:CSC17) in air under atmospheric pressure at room temperature. The microcantilever has linear dimensions $h \times w \times l = 2\,\mu m \times 50\,\mu m \times 450\,\mu m$, as shown in Fig. 1(a), and has a fundamental flexural resonance at $\Omega_0/2\pi \approx 14.12$ kHz with a quality factor of $Q \approx 63$. Because $w \gg h$, the flexural deflections in the fundamental resonance are along the thickness dimension h as shown in Fig. 1(a).

A. Optical beam deflection set up

The experimental set up is illustrated in Fig. 2. The microcantilever is glued to a rotation stage, which is fixed onto an xyz-positioning stage. A diode laser (Thorlabs Model S1FC635) with a wavelength of $\lambda = 635$ nm is used, and the optical power level in the experiment remains below 0.8 mW. The light from the diode laser is first collimated and then passed through a converging lens (125-mm focal length) to focus the light down to a 40-μm diameter optical spot. A CCD camera is used for aligning the optical spot onto the tip of the microcantilever. The spot reflects from the tip of the cantilever onto a single-element amplified photodetector (Thorlabs Model PDA8A). A knife edge is placed in front of the photodetector to block half of the light reflecting from the cantilever surface. Because of the knife edge, as the cantilever moves the power on the photodetector varies proportionally to the displacement of the cantilever tip;[20] this allows for monitoring the thermal oscillations of the cantilever with good displacement sensitivity. The optical alignment can be further verified by observing the diffraction pattern of the reflected light, produced by the microcantilever.

Because this optical transduction scheme is non-interferometric, it is not easy to obtain the transduction gain (the conversion factor for the displacement into Volts)
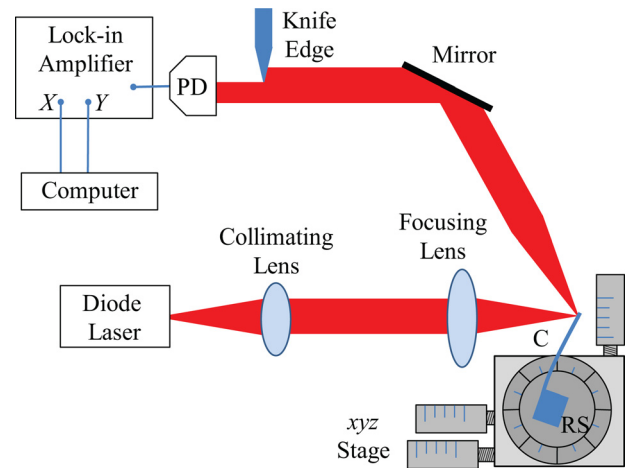

Fig. 2. Schematic of the experimental set up. Light from a diode laser is collimated and focused on the tip of a cantilever (C), which is placed on a rotation stage (RS) on top of an xyz-stage. The reflected light from the cantilever is directed onto a single-element amplified photodetector (PD). A knife edge is placed in front of the photodetector to block half of the light reflecting from the cantilever.

directly, as was done in the work of Shusteff *et al.*[4] Instead, the gain is determined by measuring the thermal noise amplitude and calibrating it against the equipartition theorem result $z_{rms}^2 = k_B T / \kappa$, with the cantilever stiffness κ calculated from elasticity considerations to be[21] $\kappa = Ewh^3/(4l^3)$, where E is the Young's modulus. For our cantilever we find $\kappa \approx 0.2\,\text{N/m}$, thus giving an overall transducer gain of $1\,\mu\text{V/pm}$.

B. Electronics

The output of the photodetector is fed into a dual-phase lock-in amplifier (Stanford Research Systems, SR 830). The lock-in reference frequency f_r and bandwidth Δf are the two variables of interest in our measurements, as well as the number of samples N. In modern digital lock-in amplifiers, one usually sets the filter time constant instead of Δf. The signal processor of the lock-in amplifier uses mathematical algorithms for computing the averages. In most cases the filter time constant is of order $1/\Delta f$. One needs to consult the lock-in amplifier manual to determine the value of Δf from the filter time constant.

For independent sampling, the sampling time τ is set to be larger than the relevant time scale in the system. The first relevant time scale is determined by the decay time of the filter. Usually, the decay time is of order the filter time constant of $\sim 1/\Delta f$. (Again, the lock-in manual can be consulted for accurate relationships between the decay time and Δf.) The second relevant time scale is the ring-down time of the microcantilever: $2\pi Q/\Omega_0 \approx 4\,\text{ms}$. In short, one needs to consider all time scales and determine the sampling time τ accordingly.

In some of our measurements described below, f_r is varied while Δf is kept constant. In others, f_r is fixed and Δf is varied. In a typical experiment, once f_r and Δf are set, the $X(t)$ and $Y(t)$ outputs from the two channels of the lock-in amplifier are sampled by a computer via GPIB. The number N of samples in the experiments varies between $100 \leq N \leq 20000$.

V. RESULTS

A. Data points in the plane

Figure 3 displays typical results from a lock-in noise measurement. The data are the outputs of the two lock-in channels, $X(t)$ and $Y(t)$, sampled every 50 ms and plotted in the xy-plane as time increases. The arrow indicates the beginning position of the random-walk of the data points. Here, $f_r = 14.12\,\text{kHz}$ and the filter bandwidth is $\Delta f = 125\,\text{Hz}$.

B. Gaussian distributions

Figure 4(a) displays results from a measurement similar to that shown in Fig. 3, with $N = 10000$ points collected. As noted above, the probability of finding a point within Δx and Δy of position (x, y) is expected to be Gaussian around zero. Indeed, the normalized histograms in Figs. 4(b) and 4(c) of the data sampled from the $X(t)$ and the $Y(t)$ outputs of the lock-in, respectively, show the expected behavior; namely, both sets have Gaussian distributions around zero mean. The standard deviations are found from fits to the distributions. The sum of the squares of the standard deviations corresponds to the variance in $z(t)$, or z_{rms}^2, within the measurement bandwidth, as discussed in Sec. II D.
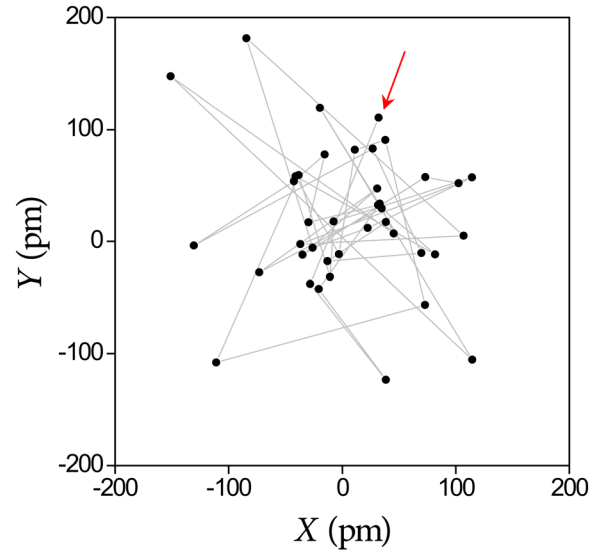

Fig. 3. Typical lock-in measurement of the in-phase and quadrature-phase components of the position of the microcantilever showing the random walk of the data points in the xy-plane. Here, $Y(t)$ is plotted against $X(t)$. The arrow indicates the beginning point of the measurement. The relevant experimental parameters are: $f_r = 14.12\,\text{kHz}$, $\Delta f = 125\,\text{Hz}$, $N = 40$, and $\tau = 50\,\text{ms}$.

The accuracy of a lock-in noise measurement depends on the number of samples in the data set considered. The more samples one uses, the closer the histograms approach to perfect Gaussians. To demonstrate this effect, we find the error δz_{rms} in z_{rms} in a fixed bandwidth of $\Delta f = 125\,\text{Hz}$ (the standard deviation of the standard deviation of the Gaussians) as a function of N. To find this error, we fit histograms with different N to Gaussians and find the error in the standard deviation from the fits. The results are shown in Fig. 4(d) with the solid line being proportional to $1/\sqrt{N}$.[5]

Figure 4(e) shows the spectral density $S_z(f)$ of the cantilever position fluctuations as measured by the lock-in amplifier. In this measurement, f_r is varied in steps of 50 Hz around the cantilever resonance frequency at a fixed bandwidth of $\Delta f = 0.42\,\text{Hz}$. A sampling time greater than the filter decay time is selected ($\tau = 4\,\text{s}$). At each frequency, the standard deviation is found from histograms of the sampled data, and the spectral density is calculated using Eq. (19) with $\Delta f = 0.42\,\text{Hz}$. In Fig. 4(e), a sharp mechanical resonance peak is clearly seen with $\Omega_0/2\pi \approx 14.12\,\text{kHz}$ and $Q \approx 63$, which are found by fitting the data to Eq. (14) (solid line). In the inset of Fig. 4(e), we show the sampled $X(t)$ and $Y(t)$ in the xy-plane at $f_r = 13.40$ and $14.12\,\text{kHz}$ (off resonance and on resonance). The larger scatter of the data points at $14.12\,\text{kHz}$ is due to the larger z_{rms}^2 at the resonance frequency.

C. Measurement bandwidth

Here, we measure z_{rms}^2 in Eq. (15) as a function of the lock-in amplifier filter bandwidth Δf. In the experiment, the lock-in amplifier reference frequency and the microcantilever resonance frequency are set to coincide: $f_r = 14.12\,\text{kHz} \approx \Omega_0/2\pi$. Then, Δf is incremented and sample sets are collected for each Δf value (varied in the range $0.4\,\text{Hz} \leq \Delta f \leq 4\,000\,\text{Hz}$). The relation between the thermal peak, f_r, and Δf is illustrated in the inset of Fig. 5. In other words, the lock-in is used as an integrator for the variance. The data
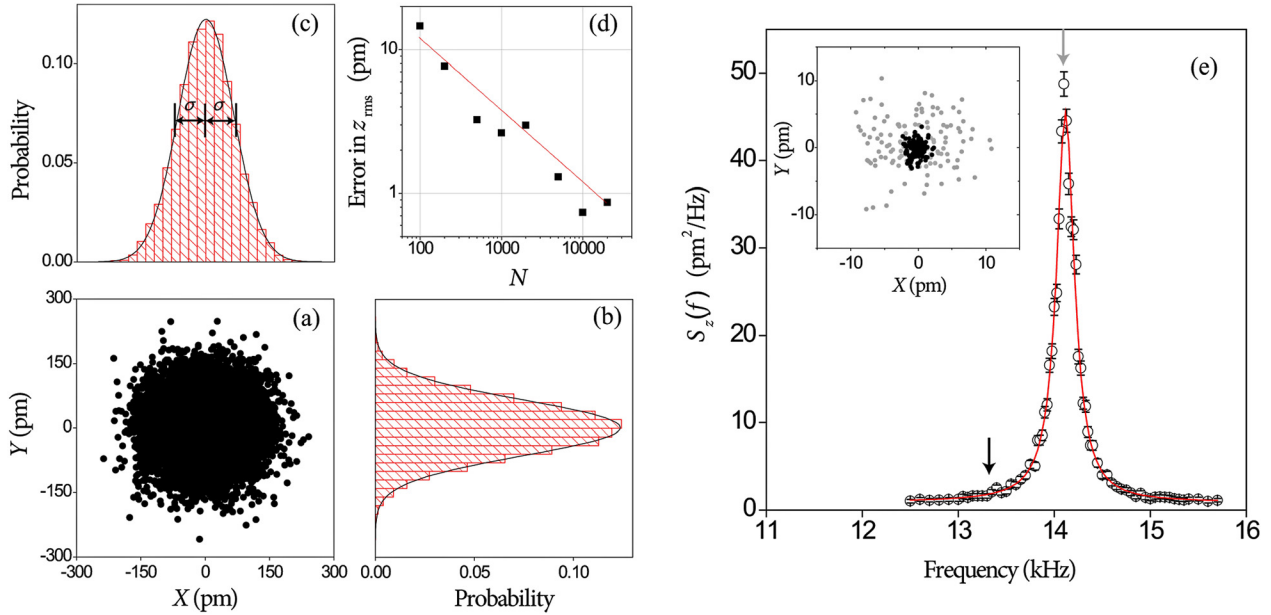
Fig. 4. Lock-in amplifier based measurements of the thermal fluctuations of a microcantilever in air. (a) The set sampled from the lock-in outputs, $X(t)$ and $Y(t)$, plotted in the plane. (b) and (c) Histograms of the samples from $X(t)$ and $Y(t)$. The solid lines are fits to normalized Gaussian probability distributions; the arrows in (c) show the standard deviation. (d) The error in the z_{rms} as a function of the number of data points N. The line shown is a fit to $1/\sqrt{N}$. Here, $f_r = 14.12$ kHz, $\Delta f = 125$ Hz, and $\tau = 50$ ms. (e) Power spectral density of the microcantilever oscillations, obtained by sweeping f_r in steps of 50 Hz around the resonance using a bandwidth $\Delta f = 0.42$ Hz. For each data point $N = 125$ samples are collected using a sampling time $\tau = 4$ s. The solid curve is a fit to Eq. (14), providing $Q \approx 63$ and $\Omega_0/2\pi \approx 14.12$ kHz. The inset shows the sampled in-phase and quadrature-phase components in the plane at an off-resonance frequency (black arrow) and on-resonance (gray arrow).

points in Fig. 5 are the results from these measurements. Returning to Eqs. (14) and (15), we can analytically integrate the expression and calculate the area under the resonance curve. For this, we take the equation of the spectral density in Fig. 4(e) with the experimentally determined $\Omega_0/2\pi$ and Q values, and integrate it as a function of Δf. Prior to this, the detection circuit noise of ~ 0.9 pm^2 for a 1-Hz bandwidth is subtracted from the total measured noise. The solid line is the result of this exercise. For a small bandwidth such that $\Delta f \ll \Omega_0/2\pi Q$, the noise power increases linearly with Δf. Once Δf becomes larger than the linewidth $\Omega_0/2\pi Q \approx 235$ Hz, the

noise power slowly saturates to the expected thermal equipartition result of $k_B T/\kappa \approx 2 \times 10^4$ pm^2.

VI. CONCLUDING REMARKS

The purpose of this article is to provide an introduction to the physics and mathematics of Gaussian thermal noise in a self-contained manner. The developed concepts are illustrated by an experiment that can be performed in the undergraduate laboratory, perhaps by using an existing AFM set up. Several different measurements, each covering different aspects of Gaussian noise and its lock-in amplifier detection, are discussed. The experiment can be improved by incorporating an optical interferometric measurement approach, which would allow for a direct calibration of the microcantilever position fluctuations against interference fringes. The lock-in-based measurement approach can be adapted for noise measurements in other systems, including electrical circuits.
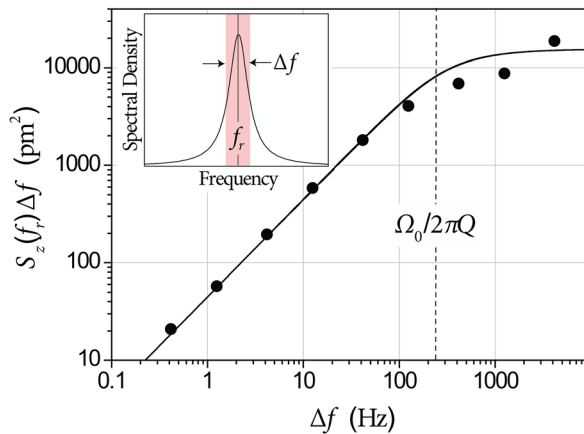
Fig. 5. The variance in the position $z_{rms}^2 = S_z(f_r)\Delta f$ measured as a function of the lock-in bandwidth Δf at the fixed reference frequency $f_r = 14.12$ kHz. The inset shows an illustration of the resonance lineshape, f_r, and Δf. The solid line is the calculated area under the resonance curve enclosed within Δf; it depends linearly on Δf for $\Delta f \ll \Omega_0/2\pi Q$ and reaches the equipartition value for $\Delta f \gg \Omega_0/2\pi Q \approx 235$ Hz.

a) Electronic mail: ekinci@bu.edu

[1] F. Reif, *Fundamentals of Statistical and Thermal Physics* (McGraw-Hill, Singapore, 1965).
[2] F. Gittes and C. F. Schmidt, "Thermal noise limitations on micromechanical experiments," Eur. Biophys. J. **27**, 75–81 (1998).
[3] Y. Kraftmakher, "Two student experiments on electrical fluctuations," Am. J. Phys. **63**, 932–935 (1995).

[4]M. Shusteff, T. P. Burg, and S. R. Manalis, "Measuring Boltzmann's constant with a low-cost atomic force microscope: An undergraduate experiment," Am. J. Phys. **74**, 873–880 (2006).

[5]R. Kubo, M. Toda, and N. Hashitsume, *Statistical Physics II: Nonequilibrium Statistical Mechanics* (Springer-Verlag, Berlin, 1995).

[6]The central limit theorem of probability is a more general statement of the Gaussian law of errors.

[7]P. Kittel, W. R. Hackleman, and R. J. Donnelly, "Undergraduate experiment on noise thermometry," Am. J. Phys. **46**, 94–100 (1978).

[8]T. J. Ericson, "Electrical noise and the measurement of absolute temperature, Boltzmann's constant and Avogadro's number," Phys. Educ. **23**, 112–116 (1988).

[9]J. C. Rodriguez-Luna and J. de Urquijo, "A simple, sensitive circuit to measure Boltzmann's constant from Johnson's noise," Eur. J. Phys. **31**, 675–679 (2010).

[10]A. Bergmann, D. Feigl, D. Kuhn, M. Schaupp, G. Quast, K. Busch, L. Eichner, and J. Schumacher, "A low-cost AFM setup with an interferometer for undergraduates and secondary-school students," Eur. J. Phys. **34**, 901–914 (2013).

[11]J. H. Scofield, "Frequency-domain description of a lock-in amplifier," Am. J. Phys. **62**, 129–132 (1994).

[12]B. G. de Grooth, "A simple model for Brownian motion leading to the Langevin equation," Am. J. Phys. **67**, 1248–1252 (1999).

[13]P. Grassia, "Dissipation, fluctuations, and conservation laws," Am. J. Phys. **69**, 113–119 (2001).

[14]D. K. C. MacDonald, "Spontaneous fluctuations," Rep. Prog. Phys. **12**, 56–81 (1949).

[15]C. V. Heer, *Statistical Mechanics, Kinetic Theory, and Stochastic Processes* (Academic Press, New York, 1972).

[16]$R(t)$ is approximated to be completely uncorrelated in time, $\langle R(t)R(s)\rangle = \sigma_R^2 \delta(t-s)$, because the impacts occur at a time scale much shorter than the particle (microcantilever) can respond.

[17]M. C. Wang and G. E. Uhlenbeck, "On the theory of the Brownian motion II," Rev. Mod. Phys. **17**, 323–342 (1945).

[18]D. E. Newland, *An Introduction to Random Vibrations, Spectral and Wavelet Analysis* (DoverPublications, New York, 2005).

[19]C. Kittel, *Elementary Statistical Physics* (John Wiley & Sons, New York, 1960).

[20]G. Meyer and N. M. Amer, "Novel optical approach to atomic force microscopy," Appl. Phys. Lett. **53**, 1045–1047 (1988).

[21]A. N. Cleland, *Foundations of Nanomechanics: From Solid-State Theory to Device Applications* (Springer-Verlag, Berlin, 2003).
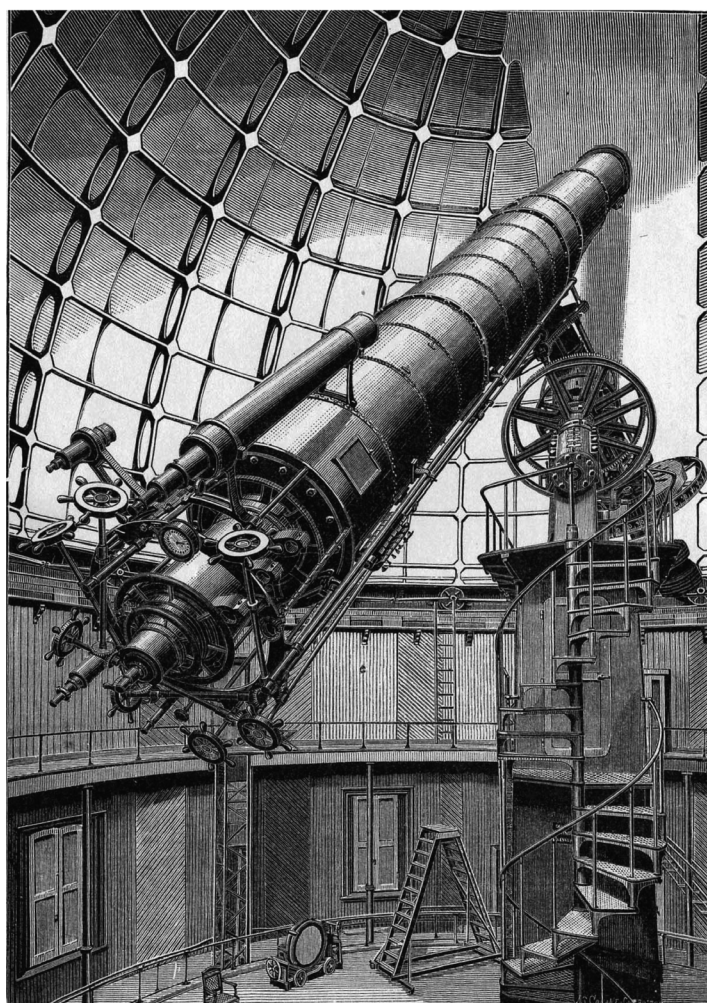
The Lick Telescope

The Lick Telescope saw first light on January 4, 1888, and this picture of it was the frontispiece of Charles A. Young's new Astronomy textbook that was published that year. The object glass was an air-spaced achromatic lens made by Alvan Clark and Sons, a Massachusetts firm that was well-known for their excellent work in optics. It aperture was 36 inches, at the time the largest in use. Nine years later the Clarks made the 40 inch Yerkes telescope, the largest useful refractor ever made. (Notes by Thomas B. Greenslade, Jr., Kenyon College)